

# Quantifying the changes in oxygen extraction fraction and cerebral activity caused by caffeine and acetazolamide

Sagar Buch<sup>1</sup>, Yongquan Ye<sup>2</sup> and E Mark Haacke<sup>1,2</sup>

## Abstract

A quantitative estimate of cerebral blood oxygen saturation is of critical importance in the investigation of cerebrovascular disease. We aimed to measure the change in venous oxygen saturation ( $Y_v$ ) before and after the intake of the vaso-dynamic agents caffeine and acetazolamide with high spatial resolution using susceptibility mapping. Caffeine and acetazolamide were administered on separate days to five healthy volunteers to measure the change in oxygen extraction fraction. The internal streaking artifacts in the susceptibility maps were reduced by giving an initial susceptibility value uniformly to the structure-of-interest, based on a priori information. Using this technique,  $Y_v$  for normal physiological conditions, post-caffeine and post-acetazolamide was measured inside the internal cerebral veins as  $Y_{\text{Normal}} = 69.1 \pm 3.3\%$ ,  $Y_{\text{Caffeine}} = 60.5 \pm 2.8\%$ , and  $Y_{\text{Acet}} = 79.1 \pm 4.0\%$ . This suggests that susceptibility mapping can serve as a sensitive biomarker for measuring reductions in cerebro-vascular reserve through abnormal vascular response. The percentage change in oxygen extraction fraction for caffeine and acetazolamide were found to be  $+27.0 \pm 3.8\%$  and  $-32.6 \pm 2.1\%$ , respectively. Similarly, the relative changes in cerebral blood flow in the presence of caffeine and acetazolamide were found to be  $-30.3\%$  and  $+31.5\%$ , suggesting that the cerebral metabolic rate of oxygen remains stable between normal and challenged brain states for healthy subjects.

## Keywords

Arterial spin labeling, brain imaging, cerebral hemodynamics, magnetic resonance imaging, neurophysiology, neurovascular coupling

Received 13 October 2015; Revised 19 February 2016; Accepted 29 February 2016

## Introduction

Being able to image the hemodynamics of the brain is key to diagnosing and understanding cerebrovascular diseases such as stroke,<sup>1–3</sup> subarachnoid hemorrhage,<sup>4</sup> vascular dementia,<sup>5,6</sup> and mild traumatic brain injury.<sup>7</sup> Two key components of brain function are oxygen extraction fraction (OEF) and cerebral metabolic rate of oxygen (CMRO<sub>2</sub>). The OEF represents the fractional amount of oxygen extracted from the arterial blood by the surrounding tissue during its passage through the capillary network. This oxygen utilization is related to brain function, which in turn regulates cerebral blood flow (CBF) and cerebral blood volume (CBV) to meet the CMRO<sub>2</sub> demand. Although positron emission tomography (PET) studies<sup>8,9</sup> have been widely used to study venous oxygen saturation ( $Y_v$ ) and CMRO<sub>2</sub> for stroke and tumor imaging,<sup>10,11</sup> PET imaging is a relatively low spatial-resolution technique and

involves injection of a radioactively labeled isotope, which requires special equipment and has risks for the patient.

The complex physiology of blood flow and oxygen saturation levels modulates the MR signal in the veins,<sup>12–15</sup> which can be detected using functional magnetic resonance imaging (fMRI) techniques through the blood-oxygen-level-dependent (BOLD) response.<sup>12,13</sup> The BOLD effect is a function of CBV, CBF, and oxygen consumed by the brain tissues.<sup>16,17</sup> Relative changes in the hemodynamic response are used

<sup>1</sup>The MRI Institute for Biomedical Research, Waterloo, Canada

<sup>2</sup>Department of Radiology, Wayne State University, Detroit, USA

## Corresponding author:

E Mark Haacke, Radiology Department, Wayne State University, Detroit, Michigan 48201, USA.

Email: nmrimaging@aol.com

as a surrogate to detect neuronal activity. MRI-based methods have been proposed to measure oxygenation in the brain, including the combination of fMRI BOLD and CBF measurements for calibrated estimates of CMRO<sub>2</sub> changes.<sup>18–21</sup> Despite its significance in the neurosciences, the BOLD technique measures relative changes and suffers from limited spatial resolution.<sup>22</sup> Furthermore, the specificity of the technique is difficult to assess because measurements may be contaminated by larger vessels representing an integrated effect from a larger territory than desired.<sup>23,24</sup> A recent alternate approach based on T<sub>2</sub> relaxation in MRI, T<sub>2</sub>-relaxation-under-spin-tagging (TRUST), allows quantification of Y<sub>v</sub> and CMRO<sub>2</sub>, but only offers measurements from a single slice placed judiciously in the brain.<sup>25</sup>

Our goal is to introduce a method that provides high-resolution, quantitative measurements of the changes in OEF in the presence of physiological challenges, particularly, the administration of vaso-dynamic agents such as caffeine and acetazolamide (brand name Diamox). Using the susceptibility maps that are generated from gradient echo phase data, the susceptibility changes and the corresponding oxygen saturation level for a given vein can be quantified.<sup>14,26,27</sup> In this article, we investigated the change in OEF based on the variation of susceptibility differences and, hence, deoxyhemoglobin levels,<sup>26,28</sup> between cerebral veins and the surrounding brain parenchyma caused by vaso-dynamic agents. Using an iterative quantitative susceptibility mapping (QSM) approach known as susceptibility weighted imaging and mapping (SWIM), we demonstrated the potential to image the hemodynamics of the brain using the vaso-dynamic agents caffeine and acetazolamide. Furthermore, to assess the effects of these vaso-dynamic agents on the CMRO<sub>2</sub>, the global and local blood flow measurements were obtained by acquiring ASL data before and after the administration of caffeine and acetazolamide. ASL is a MRI-based method that utilizes blood as a tracer by altering its magnetization using radiofrequency (RF) pulses and provides non-invasive quantification of CBF.<sup>29</sup> Based on the labeling scheme, one of the main categories of ASL techniques is pulsed ASL (PASL),<sup>30</sup> which was used in this article.

## Theory

Susceptibility maps are parametric images of relative magnetic susceptibility between tissues (such as a vein and the surrounding brain tissue) and, hence, can provide an endogenous oxygenation-dependent contrast.<sup>14</sup> Hemoglobin in red blood cells is the primary carrier of oxygen in the body and, after the tissue extracts the oxygen from it, the resulting deoxyhemoglobin appears in the venous blood. Deoxyhemoglobin is paramagnetic

due to the electron spin state of the heme iron and this is reflected in an increased susceptibility of venous blood with respect to the surrounding brain parenchyma. From the susceptibility shift ( $\Delta\chi$ ) measured using the susceptibility maps derived from the filtered-phase data, the OEF for each vessel can be quantified via:<sup>16</sup>

$$\Delta\chi = \text{Hct} \cdot \text{OEF} \cdot \Delta\chi_{\text{do}} \quad (1)$$

where  $\text{OEF} = (Y_a - Y_v)$ ,  $\Delta\chi_{\text{do}} = 0.27$  ppm (in cgs units) is the susceptibility difference between fully deoxygenated and fully oxygenated blood and Hct is the hematocrit. Assuming the arterial oxygen saturation Y<sub>a</sub> is known (here, we use Y<sub>a</sub> = 98%), Y<sub>v</sub> can be measured.

## Materials and methods

### Forced iterative susceptibility weighted imaging and mapping (FIT-SWIM)

QSM is a means to monitor iron levels in tissue and can be used to monitor oxygen saturation.<sup>14,27,31,32</sup> Our own approach, referred to as iterative SWIM has proven to be effective in reducing streaking artifacts in the brain and in improving the susceptibility values as well,<sup>27</sup> however, the streaking artifacts inside the structure-of-interest are still carried forward in the iterations. One way to reduce these artifacts is to set the susceptibility within the structure to a uniform value before applying the iterative algorithm. The idea here is to remove the effect of the streaking artifacts inside the veins by assigning a uniform initial value, which is based on our a priori knowledge about the susceptibility of the deoxyhemoglobin blood. The critical issue here is whether this will still allow the process to converge to the correct susceptibility value despite setting it to an initial empirical assumption. The concept of using a uniform initial value in FIT-SWIM was tested using a 3D brain model consisting of basal ganglia and mid brain structures, gray matter, white matter, and veins. A 3D brain susceptibility model was generated by assigning susceptibilities to various structures in the brain. By using the forward modeling approach, phase information was constructed.<sup>33–35</sup> The susceptibility maps were then generated from the resulting phase maps using the iterative SWIM algorithm with and without setting the initial susceptibility values of 0.30, 0.45, 0.70, and 1.0 ppm constant inside the veins. The veins were assigned a uniform value only for the first iteration; and the subsequent iterations were carried out conventionally.

### Inducing the physiological challenges

We compared the susceptibility maps before and after ingestion of a 200 mg NoDoz pill for caffeine (Novartis

Consumer Health Inc, Parsippany, NJ, USA) and 1000 mg administered intravenously for acetazolamide (Sagent Pharmaceuticals, Schaumburg, IL, USA) to examine the changes in oxygenation levels in the veins. Caffeine is a vasoconstrictive agent and reduces CBF and so the OEF subsequently increases,<sup>36–43</sup> while acetazolamide is a vasodilating agent and leads to an increase in CBF and so the OEF decreases.<sup>44–47</sup> Subjects were scanned twice with caffeine and acetazolamide doses administered on two different days separated by at least 1 week. The subjects were instructed not to consume any food, drug, or beverage containing caffeine 24 h prior to the scan, and not to have any meal 2 h prior to the scan.

### Selection of echo time (TE) for phase-susceptibility measurements

Susceptibility of the structure-of-interest is one of the major factors in selecting the TE. There is a trade-off involved between higher phase SNR at longer TEs versus less  $T_2^*$  signal decay and less phase wrapping at shorter TEs. As a compromise, we used a TE of 15 ms for the 3T acquisition to avoid phase wrapping between the vessel and background tissue, while maintaining a maximum expected phase difference of 2–3 radians for the physiological range of  $Y_v$  (50–75%).<sup>31</sup>

### Data acquisition

Susceptibility weighted imaging (SWI) data<sup>26,28,48</sup> were acquired once before the intake of acetazolamide or caffeine and then every 15 min for four time points after the intake.<sup>48,49</sup> Acquiring data at different time points was essential to study the variation in susceptibility values based on the functional dynamics caused by the drug and to select the time point that provided the peak change. The study was approved by the institutional review board of Wayne State University, Detroit, MI, and performed in accordance with the ethical guidelines of the Declaration of Helsinki. After a thorough explanation of the study, written informed consent was obtained from seven healthy volunteers. All the SWI data were acquired using a radio-frequency (rf)-spoiled, fully flow compensated 3D sequence with the imaging parameters: TE = 15 ms, FA = 13°, TR = 24 ms, BW = 119 Hz/pixel, voxel size = 0.5 × 0.5 × 0.5 mm<sup>3</sup>, and matrix size = 448 × 336 on a 3T Verio scanner (Siemens Healthcare, Erlangen, Germany). For the first five volunteers, the product PASL<sup>50</sup> sequence from Siemens was used for CBF analysis. QUIPSS II (quantitative imaging of perfusion using a single subtraction, version 2), thin slice TI<sup>1</sup>, periodic saturation (Q2TIPS) with the proximal inversion with a control for off-resonance effects (PICORE) scheme was utilized

with inversion time delays of TI<sub>1</sub> = 700 ms (time between the inversion pulse and the beginning of periodic saturation pulses), TI<sub>1s</sub> = 1600 ms (time between the inversion pulse and the end of periodic saturation pulses), TI<sub>2</sub> = 1800 ms (time between the inversion pulse and acquisition of the proximal image), and imaging parameters: TE/TR = 18 ms/3500 ms, FA = 18°, voxel size = 3.5 × 3.5 × 3.5 mm<sup>3</sup> and BW = 2441 Hz/pixel.<sup>51,52</sup> Interleaved label and control images were acquired using a gradient-echo single shot EPI readout.

### Image processing

The original phase images were unwrapped using the Laplacian method,<sup>53,54</sup> followed by background field removal using sophisticated harmonic artifact reduction for phase (SHARP)<sup>55</sup> to generate the processed phase map at TE = 15 ms. The signal-to-noise ratio (SNR) in the magnitude images was estimated as the ratio of mean over standard deviation of values measured within a homogeneous region of white matter. By using the arterial binary mask generated from the magnitude data, the flow artifacts inside the arteries were suppressed.<sup>56</sup> The proposed method of FIT SWIM (initial value of 0.45 ppm for veins) was used to produce the local susceptibility distribution maps.

The susceptibility distribution was measured inside the major cerebral veins: right and left internal cerebral veins (ICVs), right and left thalamo-striate veins, right and left septal veins, vein of Galen and straight sinus. The change in susceptibility between the normal brain state ( $\Delta\chi_{\text{Normal}}$ ) and post-drug or active ( $\Delta\chi_{\text{Active}}$ ) state was used to quantify the effect on the tissue oxygen consumption variation ( $\Delta\text{OEF}$ ), based on equation (1):

$$\frac{\Delta\text{OEF}}{\text{OEF}_{\text{Normal}}} = \frac{\Delta\chi_{\text{Active}} - \Delta\chi_{\text{Normal}}}{\Delta\chi_{\text{Normal}}} \quad (2)$$

The CBF maps were calculated according to the formula from Wang et al. (2003), where we assumed longitudinal relaxation time for blood ( $T_{1b}$ ) = 1650 ms,  $\lambda$  = blood/tissue water partition coefficient = 0.9 g/ml and inversion efficiency,  $\alpha$  = 0.95.<sup>57</sup> Whole brain gray matter maps used to measure mean CBF values were produced using statistical parametric mapping (SPM) 12 (Wellcome Trust Centre for Neuroimaging, University College of London, UK) implemented in Matlab (Mathworks Inc., USA).

### Statistical analysis

Paired-sample t-tests were performed to assess the differences in FIT-SWIM before and after the caffeine or acetazolamide challenge across the subjects. The p values of less than 0.05 were used to indicate statistical

significance. All data are expressed as mean  $\pm$  standard deviation.

## Results

### Numerical simulations

The ability of FIT-SWIM to reduce internal streaking artifacts for the straight sinus compared with the conventional iterative SWIM method is shown in Figure 1. The mean and standard deviation of the susceptibility distribution inside the straight sinus was measured as  $\Delta\chi = 0.41 \pm 0.04$  ppm for the conventional method, whereas the measured susceptibility distribution was found to be  $\Delta\chi = 0.45 \pm 0.01$  ppm and  $\Delta\chi = 0.46 \pm 0.02$  ppm when taking the initial values as 0.45 ppm and 0.70 ppm inside the veins, respectively, for FIT-SWIM.

Figure 1(a) and (b) demonstrates that, independent of the choice of the initial value, the mean susceptibility value inside the straight sinus stays at or approaches the correct susceptibility value of 0.45 ppm. This is expected as only a small cone of k-space elements is modified (regularization threshold = 0.1), whereas the other remaining k-space components outside the cone of singularity help drive the value back to the true susceptibility. When the initial value of 0.45 ppm was used, the iterative results were the best in terms of the highest accuracy in the mean susceptibility value (0.453 ppm) and the lowest standard deviation (0.013 ppm). With no constraint on the values inside the straight sinus, the final measured susceptibility value was 0.446 ppm inside the straight sinus, but the standard deviation increased to 0.038 ppm due to the streaking artifacts.

### In vivo data analysis

The SNR of the gradient echo magnitude images was measured as  $\text{SNR}_{\text{mag}} = 17.8 \pm 2.1$ . Similar to the numerical simulations, the results from the in vivo data (Figure 1(c) to (f)) demonstrate the improvement in the susceptibility reconstruction of the veins. The susceptibility value inside the straight sinus, without initial constraints, was measured to be  $0.41 \pm 0.14$  ppm. On the other hand, when the starting value of 0.45 ppm was assigned, the susceptibility inside the straight sinus increased to  $0.45 \pm 0.06$  ppm. Likewise, the susceptibility of a small peripheral vein improved from  $0.32 \pm 0.09$  ppm to  $0.36 \pm 0.04$  ppm (the vein is identified by the white arrows in Figure 1(e) and (f)). After caffeine intake, there is a clear increase in the susceptibility of venous blood, as can be seen from the brighter venous vessels in Figure 2(a) and (c), indicating an increase in deoxyhemoglobin level. On the other hand, after acetazolamide, there is a clear decrease in

the susceptibility of venous blood, as can be seen from the less bright venous vessels in Figure 2(b) and (d), indicating a decrease in deoxyhemoglobin. The profile plots across the ICVs (black line in Figure 2(e) to (h)) demonstrate the effects of caffeine/acetazolamide intake on susceptibility (Figure 2(i)).

For the caffeine and acetazolamide tests, the measured susceptibility values inside the ICVs, are shown in Table 1. The susceptibility value reaches the peak after the second time point, and remains consistent for the third and the fourth time points. Hence, we selected the second time point (30 min after dose administration) to analyze the post-drug intake functional state.

Histograms of the mean GM CBF values before and after the intake of acetazolamide, for one healthy volunteer are shown in Figure 3. Whole brain GM mean CBF was measured during caffeine administration as pre CBF = 46.5 ml/100 g of tissue/min and post CBF = 32.4 ml/100 g of tissue/min. Similarly, for acetazolamide administration, pre CBF = 51.4 ml/100 g of tissue/min and post CBF = 67.7 ml/100 g of tissue/min. Hence, the relative change in the whole brain mean CBF in the presence of caffeine and acetazolamide was calculated as  $(\Delta\text{CBF}_{\text{caffeine}})/(\text{CBF}_{\text{caffeine}}) \approx -30.3\%$  and  $(\Delta\text{CBF}_{\text{Acet}})/(\text{CBF}_{\text{Acet}}) \approx +31.5\%$ . The CBF maps before and after the caffeine and acetazolamide administration and their respective susceptibility maps are shown in Figure 4. In addition, the regional measurements surrounding major veins provide a direct comparison with our SWIM values acquired from these major veins. The areas for regional CBF measurements are highlighted in Figure 4(f) and (g). The regional CBF values are stated in Figure 5 alongside the susceptibility mapping results.

As shown in Figure 5(a), compared with the pre-caffeine values, there is a statistically significant increase in susceptibility inside the ICVs ( $\Delta\chi_{\text{Caffeine-Normal}} = +0.15 \pm 0.04$  ppm;  $p < 0.01$ ) at 30-min post-caffeine. Similarly, the post-acetazolamide results showed a statistically significant decrease in the measured susceptibility inside the ICVs ( $\Delta\chi_{\text{Acet-Normal}} = -0.14 \pm 0.05$  ppm;  $p < 0.01$ ). Assuming  $\Delta\chi_{\text{do}} = 0.27$  ppm (cgs) and Hct = 44% in equation (1), the venous oxygen saturation level (inside the ICVs) for normal physiological conditions, post-caffeine, and post-acetazolamide for the first volunteer were calculated as (mean  $\pm$  standard deviation):  $Y_{\text{Normal}} = 69.1 \pm 3.3\%$ ,  $Y_{\text{Caffeine}} = 60.5 \pm 2.8\%$ , and  $Y_{\text{Acet}} = 79.1 \pm 4.0\%$ . The inter-subject error in mean values of venous oxygen saturation over the five subjects was measured inside the ICVs as:  $\sigma_{Y, \text{Normal}} = \pm 0.7\%$ ,  $\sigma_{Y, \text{Caffeine}} = \pm 1.2\%$ ,  $\sigma_{Y, \text{Acet}} = \pm 1.2\%$ . For the caffeine challenge, the percentage change in OEF from pre to post caffeine was (mean  $\pm$  inter-subject variability)  $+27.0 \pm 3.8\%$ ; and for the acetazolamide challenge, the percentage change in OEF from pre to post was

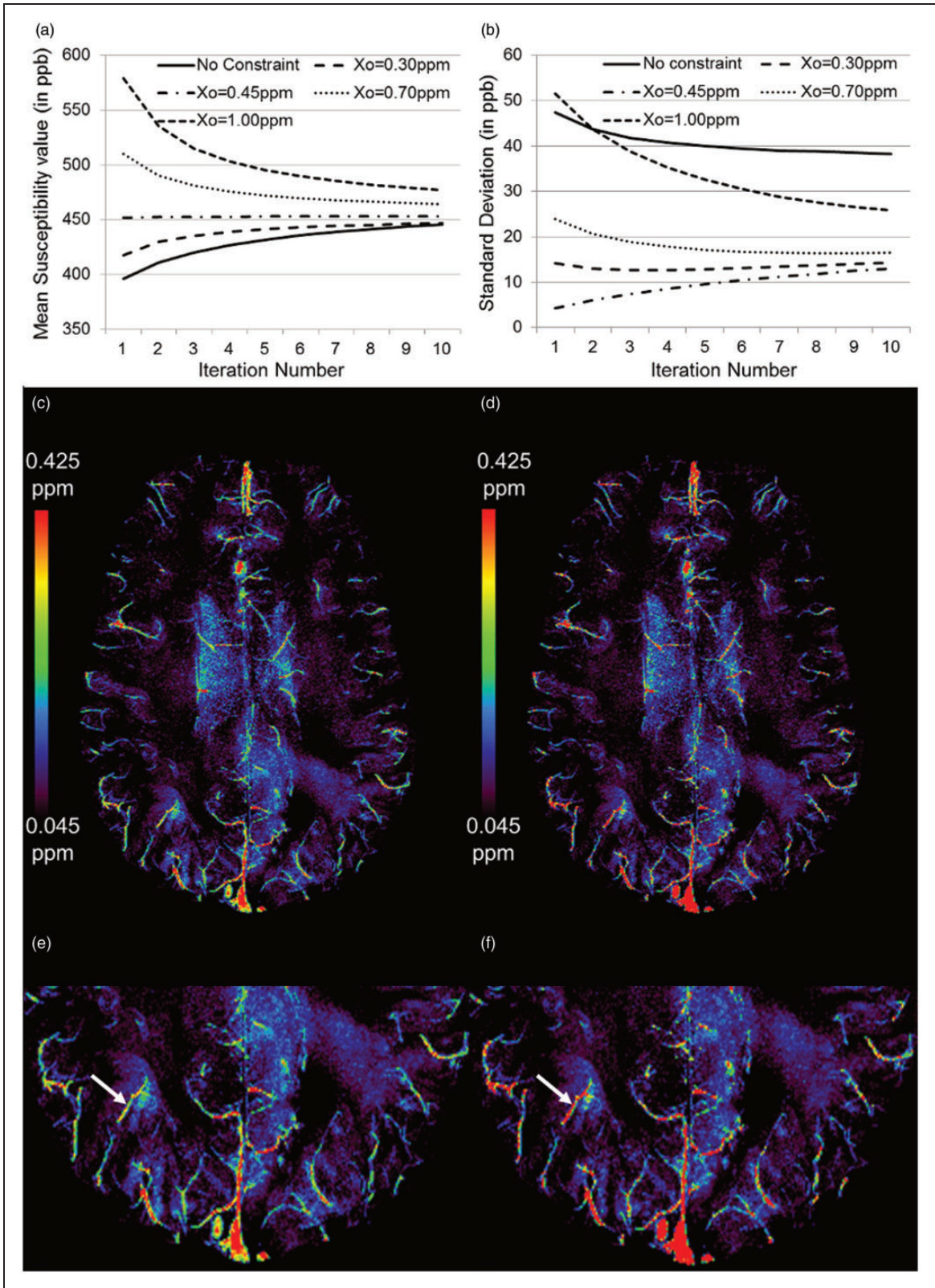


**Figure 1.** Mean (a) and standard deviation (b) of the susceptibility measured inside the straight sinus at each iteration of the FIT-SWIM algorithm. Different initial values ( $\chi_0$ ) were set inside the veins. Independent of the choice of starting point, the values tended to converge close to the expected susceptibility of 0.45 ppm. The use of a suitable initial value, based on the a priori knowledge of the susceptibility of the structure-of-interest, reduces the streaking artifacts inside the veins. (c) Susceptibility map of an in vivo data from a healthy volunteer generated using the conventional iterative technique, and (d) susceptibility map of the same data generated using FIT-SWIM. Note the improvement in the susceptibility distribution (identified by white arrows in (e) and (f)), inside the veins of different sizes, in (f) with respect to the conventional iterative SWIM results in (e).

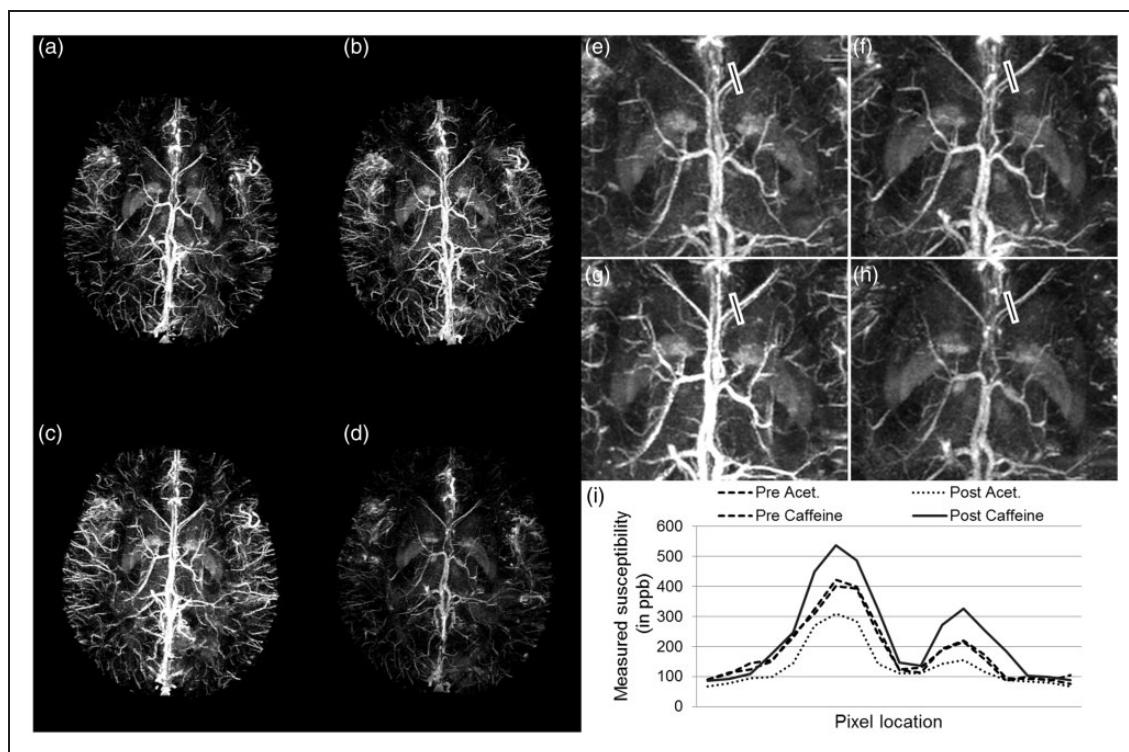


**Figure 2.** Evaluation of dynamic changes in venous susceptibility distribution due to the administration of caffeine and acetazolamide. Phase data were acquired 4 times after the drug ingestion/infusion, at an interval of 15 min. Maximum intensity projection (MIP) of susceptibility maps for the data acquired before (a) caffeine and (b) acetazolamide intake, respectively, (c) MIP of susceptibility maps for the data at the second time point (30 min) after caffeine intake, (d) MIP of susceptibility maps at the second time point (30 min) after acetazolamide intake. MIP images were generated from susceptibility maps over 32 slices or 16 mm in the slice-select direction. (e) to (h) represent zoomed insets of images (a) to (d), respectively. The profile plot (i) demonstrates the variation in susceptibility values across the septal veins, along the black lines shown in (e) to (h), caused by these altered brain states.

**Table 1.** Measured susceptibility values inside the internal cerebral veins before and at four time points (at intervals of 15 min) after caffeine and acetazolamide administration.

	Pre-administration (in ppm)	Post-administration (in ppm)			
		Time 1	Time 2	Time 3	Time 4
Caffeine	0.47 ± 0.06	0.53 ± 0.07	0.58 ± 0.10	0.61 ± 0.08	0.61 ± 0.09
Acetazolamide	0.46 ± 0.08	0.38 ± 0.09	0.36 ± 0.06	0.36 ± 0.08	0.37 ± 0.07

−32.6 ± 2.1% for the right ICVs (see Table 2 for the change in OEF measurements in major veins).

## Discussion

In this article, we have proposed a new QSM approach referred to as FIT-SWIM to reduce streaking artifacts by forcing susceptibility values to be uniform in the first iteration of the iterative SWIM approach. This method was then used to quantify in vivo local OEF changes in the brain in the presence of both caffeine and acetazolamide. The iterative SWIM approach itself has been

used previously to evaluate contralateral changes in OEF in stroke by evaluating the presence of asymmetrically prominent cortical veins (APCV).<sup>1</sup> These changes have been ascribed to hypo-perfusion that leads to an effective OEF increase while the usual level of oxygen metabolism is maintained.

We have demonstrated that FIT-SWIM, even when using the constant phase constraint for just the first iteration, reduced not only the external streaking artifacts but also the streaking inside the veins. The plots shown in Figure 1(a) and (b) show that the method is robust against the errors made in assuming the initial

phase value, as the measured susceptibility value converges toward the actual value. However, the closer the assumed value to the actual value, the faster the convergence. Hence, it is advantageous to have a priori

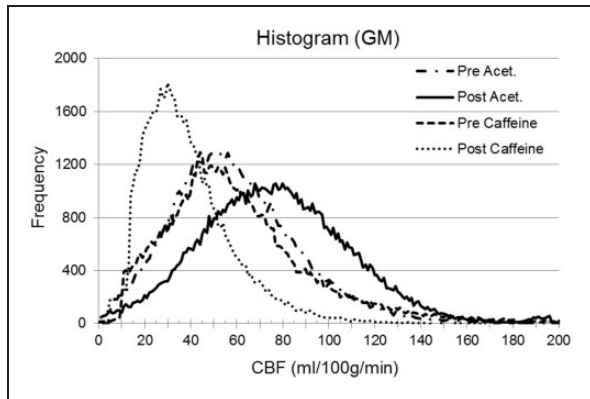


**Figure 3.** The histogram of the gray-matter (GM) mean CBF values generated from pulsed ASL (PASL) data of one healthy volunteer. Caffeine and acetazolamide were administered on separate days. GM mean CBF values in ml/100 g/min:  $CBF_{Normal} = 51.4$ ,  $CBF_{Caffeine} = 32.1$ , and  $CBF_{Acet} = 67.7$ .

information of the susceptibility value for the structure-of-interest. Consistent with the simulated results, the susceptibility maps reconstructed from the in vivo data (Figure 1(c) to (f)) using FIT-SWIM showed improvement over the conventional iterative SWIM. As part of the general processing, we also removed phase from the arteries to further reduce streaking artifacts from incomplete flow compensation.<sup>56</sup>

In addition to measuring the oxygen saturation in a normal brain state, it can be useful to invoke special physiological challenges, such as vasodilation or vasoconstriction, to determine the state of autoregulation or cerebral vascular reserve. Caffeine-related antagonism reduces the ability of adenosine to contribute to functional increases in CBF.<sup>36,40,41,58</sup> Since brain activity appears to remain constant, the decrease of CBF in the presence of caffeine should lead to an increase of OEF when  $CMRO_2$  is constant. The increased OEF would lead to an increase of deoxyhemoglobin in the venous blood; therefore, we expect to see higher susceptibility values in the post caffeine case.<sup>59</sup> This is validated in our study where it is clear that caffeine caused a decrease in the venous oxygen saturation levels, inside the ICVs from normal ( $Y_{Normal} = 69.1 \pm 3.3\%$ ) to post-

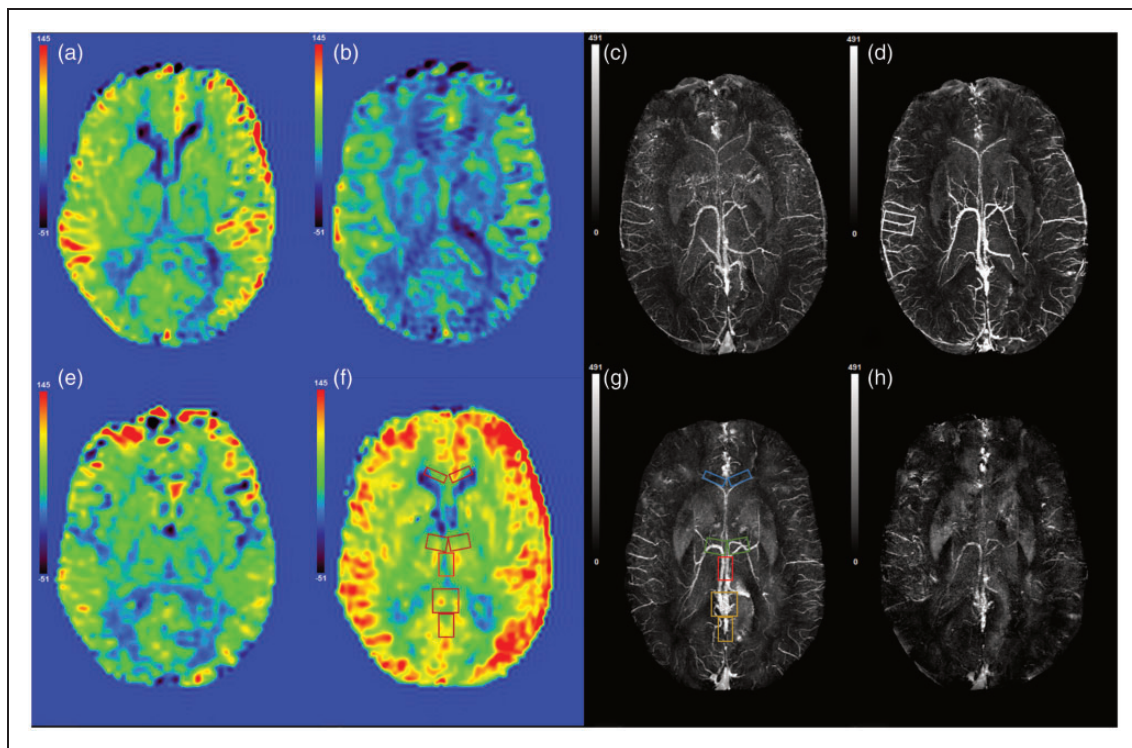


**Figure 4.** CBF maps (a) before and (b) after the intake of caffeine. Susceptibility maps (c) before and (d) after the intake of caffeine. Similarly, (e), (f) and (g), (h) are CBF and susceptibility maps before and after acetazolamide administration. The areas measured for regional CBF values are highlighted in (g) as right and left internal cerebral veins = red; right and left thalamo-striate veins = green; right and left septal veins = blue; vein of Galen and straight sinus = orange.

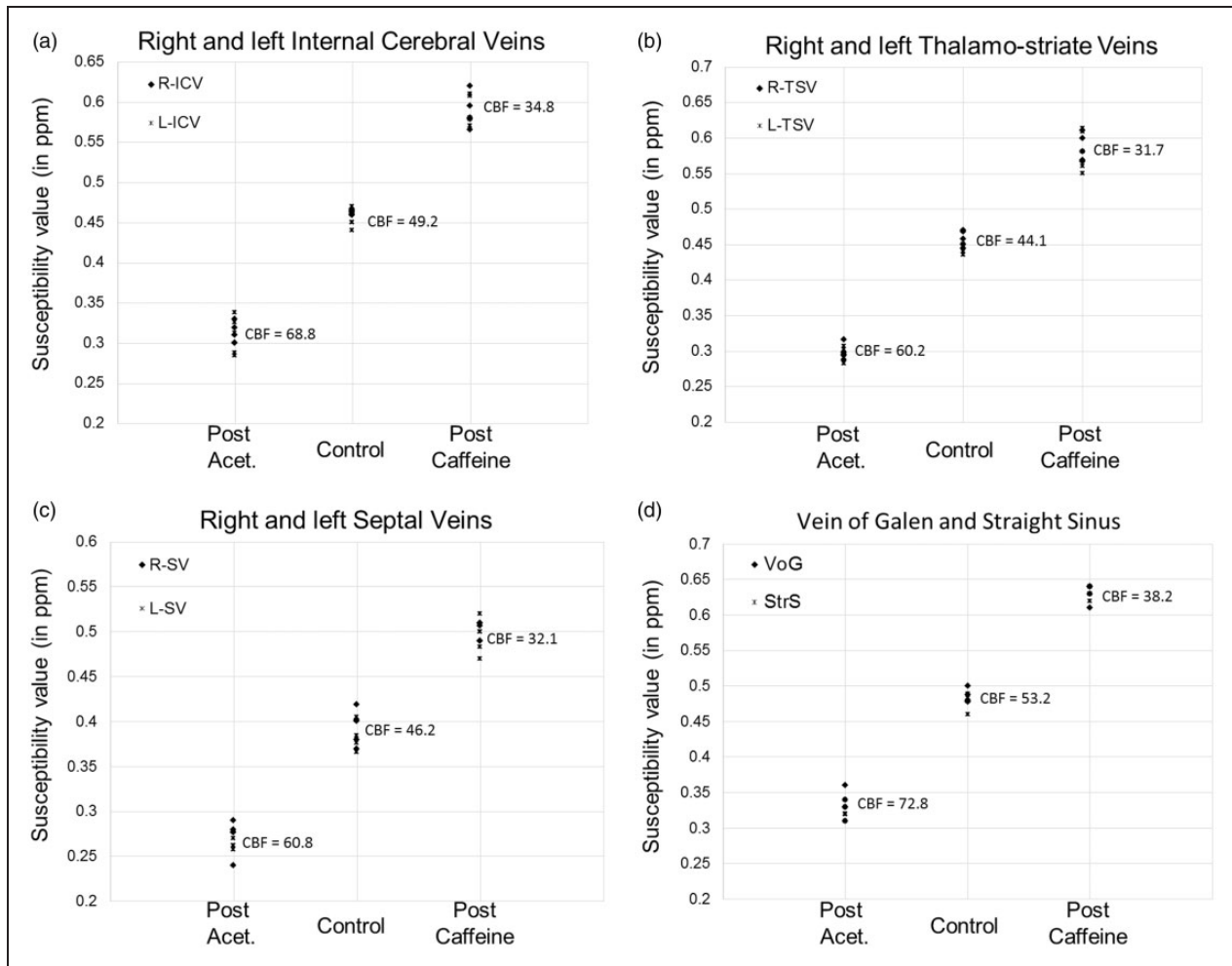


**Figure 5.** Susceptibility values measured inside the major cerebral veins across five healthy volunteers: (a) right and left internal cerebral veins (R-ICV, L-ICV); (b) right and left thalamo-striate veins (R-TSV, L-TSV); (c) right and left septal veins (R-SV, L-SV); and (d) vein of Galen (VoG) and straight sinus (StrS). The phase data were acquired before and after the administration of acetazolamide and caffeine with TE = 15 ms and a voxel resolution = (0.5 mm<sup>3</sup>). Each drug test was performed on separate days. The susceptibility values generated from the data acquired pre-administration of these drugs were averaged. The mean regional CBF values (in ml/100 g of tissue/min) surrounding these major veins are stated for each vaso-dynamic brain state.

caffeine ( $Y_{\text{Caffeine}} = 60.5 \pm 2.8\%$ ). Similarly, the increase in venous oxygen saturation in the presence of the vaso-dilating agent, acetazolamide ( $Y_{\text{Acet}} = 79.1 \pm 4.0\%$ ), is also within our expectations. Furthermore, these results are in good agreement with previous studies on caffeine.<sup>14,60–62</sup> Results of the acetazolamide challenge are close to the previously measured value for carbogen intake  $Y_{\text{carbogen}} = 80\%$  ( $\Delta\chi_{do} = 0.27$  ppm).<sup>60</sup>

Some of the limitations of this study include limited resolution, the use of estimates for hematocrit and arterial oxygen saturation, and possible habituation for caffeine drinkers. Ideally, the measured variation should reflect the exact physiological alterations in the local venous vasculature where oxygen exchange between the cerebral vessels and tissue occurs during

neural activation. In reality, the sensitivity in the smaller veins is confounded by the partial volume effect due to the limited resolution. There is much room for improvement in resolution by introducing fast imaging techniques such as compressed sensing.<sup>63–65</sup>

To calculate the venous oxygen saturation levels, several physiological parameters such as arterial oxygenation saturation level ( $Y_a$ ) and total hemoglobin concentration (Hct) are, in general, assumed constant among subjects. However, hematocrit values are dependent on the age and sex of the subject with normal levels ranging from 40.7% to 50.3% for males and 36.1% to 44.1% for females.<sup>66</sup> Making an assumption about the hematocrit will clearly impact the exact value of the estimated oxygen saturation. Therefore,



**Table 2.** Mean  $\pm$  inter-subject variability of the percentage change in oxygen extraction fraction for cerebral veins of different vessel sizes, across five healthy subjects, measured before and after administration of acetazolamide and caffeine.

Vein	$\frac{\Delta\text{OEF}_{\text{Acet}}}{\text{OEF}_{\text{Pre-Acet}}}$ %	$\frac{\Delta\text{OEF}_{\text{Caffeine}}}{\text{OEF}_{\text{Pre-Caffeine}}}$ %	Vein	$\frac{\Delta\text{OEF}_{\text{Acet}}}{\text{OEF}_{\text{Pre-Acet}}}$ %	$\frac{\Delta\text{OEF}_{\text{Caffeine}}}{\text{OEF}_{\text{Pre-Caffeine}}}$ %
R-ICV	$-32.6 \pm 2.1\%$	$+27.0 \pm 3.8\%$	L-ICV	$-31.7 \pm 5.1\%$	$+29.9 \pm 3.2\%$
R-TSV	$-34.9 \pm 3.1\%$	$+27.8 \pm 6.4\%$	L-TSV	$-34.1 \pm 3.1\%$	$+30.4 \pm 5.1\%$
R-SV	$-30.7 \pm 6.1\%$	$+27.4 \pm 7.4\%$	L-SV	$-31.1 \pm 3.6\%$	$+28.1 \pm 8.1\%$
VoG	$-31.1 \pm 4.7\%$	$+30.3 \pm 2.5\%$	StrS	$-32.0 \pm 2.4\%$	$+32.0 \pm 2.4\%$

R-ICV, L-ICV: right and left internal cerebral veins; R-TSV, L-TSV: right and left thalamo-striate veins; R-SV, L-SV: right and left septal veins; VoG: vein of Galen; StrS: straight sinus.

our strategy was to estimate the percentage change in OEF values before and after the drug intake instead of its absolute value, which is independent of Hct.

Monitoring CMRO<sub>2</sub> to see if it remains the same after these challenges requires CBF measurements,<sup>67,68</sup> as CMRO<sub>2</sub> is proportional to the product of OEF and CBF. A reduction of CBF by 30% was observed in response to caffeine intake, which is in good agreement with the previous studies.<sup>37,69–71</sup> The change in oxygen saturation has been previously shown to be related to CBF changes:<sup>28</sup>  $|\Delta Y/(1-Y)| \approx |\Delta\text{CBF}/\text{CBF}|$ . From our QSM results, for caffeine and acetazolamide experiments:  $\Delta Y_{\text{caffeine}} = 0.09$  [ $|\Delta Y_{\text{caffeine}}/(1-Y_{\text{Normal}})| = 30\%$ ] suggests that the CMRO<sub>2</sub> remains stable between normal and challenged brain states for a healthy subject. This uncoupling of CBF and CMRO<sub>2</sub> is consistent with caffeine acting primarily on adenosine receptors to constrict blood vessels and reduce CBF, with a considerably weaker effect on energy metabolism.<sup>72</sup> The decrease in CBF is therefore revealed by increased OEF, in agreement with recent studies on the effect of caffeine on CMRO<sub>2</sub>.<sup>72,73</sup> In addition, the CMRO<sub>2</sub>-CBF uncoupling is also observed for acetazolamide administration, where an increase in CBF by 32% is accompanied by the decrease in oxygen fraction,  $\Delta Y_{\text{Acet}} = 0.1$  [ $|\Delta Y_{\text{Acet}}/(1-Y_{\text{Acet}})| = 33.3\%$ ]. Previous PET studies have shown either no significant effect of acetazolamide on CMRO<sub>2</sub> and neuronal activity<sup>74</sup> or at best a slightly decreased CMRO<sub>2</sub>.<sup>44</sup> This effect of acetazolamide on CBF is probably explained by a decrease in brain pH rather than by brain tissue hypoxia due to inhibition of oxygen unloading in the brain capillaries.

As for potential habituation effects for heavy coffee drinkers, Field et al. (2003) reported a higher caffeine-induced response, i.e. CBF reduction, in heavy caffeine users (>300 mg/day).<sup>71</sup> Consequently, the susceptibility values of veins should be larger as well. However, they investigated the subjects after more than 30 h of caffeine deprivation, when typical withdrawal symptoms, such as headache and fatigue, reach a maximum in intensity.<sup>58</sup> In contrast to their study design, we did not recruit heavy caffeine users. We consider it a more

realistic scenario that the users are not in a state of severe withdrawal when the subjects refrain from caffeine intake 24 h prior to the scan.

In conclusion, this article demonstrated an improvement in iterative SWIM using FIT-SWIM for susceptibility mapping and showed that there appears to be decoupling between flow effects and CMRO<sub>2</sub> by using both FIT-SWIM and CBF changes as measured with ASL. Further, the vascular effects of acetazolamide and caffeine, in normal human subjects, were proven to be large enough to be easily measured. Therefore, this susceptibility difference could serve as a sensitive biomarker for measuring cerebro-vascular reserve in stroke and other diseases.

### Funding

The author(s) disclosed receipt of the following financial support for the research, authorship, and/or publication of this article: This work was supported in part by the Department of Defense through award DOD/USAMRAA W81XWH-12-1-0522 and by the National Institutes of Health (NIH) (grant number R21NS090153).

### Acknowledgments

The views, opinions, and/or findings contained in this report are those of the author(s) and should not be construed as an official government position, policy or decision unless so designated by other documentation.

### Declaration of conflicting interests

The author(s) declared no potential conflicts of interest with respect to the research, authorship, and/or publication of this article.

### Authors' contributions

SB, YY, and EMH: project design; SB: data processing, analysis, manuscript drafting and revising; YY: subject recruitment and data acquisition; EMH: critiquing and final approval.

### References

1. Xia S, Utriainen D, Tang J, et al. Decreased oxygen saturation in asymmetrically prominent cortical veins in

- patients with cerebral ischemic stroke. *Magn Reson Imaging* 2014; 32: 1272–1276.
2. Geisler BS, Brandhoff F, Fiehler J, et al. Blood-oxygen-level-dependent MRI allows metabolic description of tissue at risk in acute stroke patients. *Stroke* 2006; 37: 1778–1784.
  3. Siemonsen S, Fitting T, Thomalla G, et al. T<sub>2</sub>' imaging predicts infarct growth beyond the acute diffusion-weighted imaging lesion in acute stroke. *Radiology* 2008; 248: 979–986.
  4. Wu Z, Li S, Lei J, An D, et al. Evaluation of traumatic subarachnoid hemorrhage using susceptibility-weighted imaging. *Am J Neuroradiol* 2010; 31: 1302–1310.
  5. Ayaz M, Boikov AS, Haacke EM, et al. Imaging cerebral microbleeds using susceptibility weighted imaging: one step toward detecting vascular dementia. *J Magn Reson Imaging* 2010; 31: 142–148.
  6. Frackowiak RS, Pozzilli C, Legg NJ, et al. Regional cerebral oxygen supply and utilization in dementia. A clinical and physiological study with oxygen-15 and positron tomography. *Brain J Neurol* 1981; 104: 753–778.
  7. Doshi H, Wiseman N, Liu J, et al. Cerebral hemodynamic changes of mild traumatic brain injury at the acute stage. *PLoS One* 2015; 10: e0118061.
  8. Schelbert HR. Blood flow and metabolism by PET. *Cardiol Clin* 1994; 12: 303–315.
  9. Leenders KL, Perani D, Lammertsma AA, et al. Cerebral blood flow, blood volume and oxygen utilization. *Brain* 1990; 113: 27–47.
  10. Sobesky J, Zaro Weber O, Lehnhardt FG, et al. Does the mismatch match the penumbra? Magnetic resonance imaging and positron emission tomography in early ischemic stroke. *Stroke* 2005; 36: 980–985.
  11. Miles KA and Williams RE. Warburg revisited: imaging tumour blood flow and metabolism. *Cancer Imaging* 2008; 8: 81–86.
  12. Ogawa S, Lee TM, Kay AR, et al. Brain magnetic resonance imaging with contrast dependent on blood oxygenation. *Proc Natl Acad Sci USA* 1990; 87: 9868–9872.
  13. Ogawa S, Menon RS, Tank DW, et al. Functional brain mapping by blood oxygenation level-dependent contrast magnetic resonance imaging. A comparison of signal characteristics with a biophysical model. *Biophys J* 1993; 64: 803–812.
  14. Haacke EM, Tang J, Neelavalli J, et al. Susceptibility mapping as a means to visualize veins and quantify oxygen saturation. *J Magn Reson Imaging* 2010; 32: 663–676.
  15. Kwong KK, Belliveau JW, Chesler DA, et al. Dynamic magnetic resonance imaging of human brain activity during primary sensory stimulation. *Proc Natl Acad Sci USA* 1992; 89: 5675–5679.
  16. Haacke EM, Lai S, Reichenbach JR, et al. In vivo measurement of blood oxygen saturation using magnetic resonance imaging: a direct validation of the blood oxygen level-dependent concept in functional brain imaging. *Hum Brain Mapp* 1997; 5: 341–346.
  17. Rauscher A, Sedlacik J, Barth M, et al. Noninvasive assessment of vascular architecture and function during modulated blood oxygenation using susceptibility weighted magnetic resonance imaging. *Magn Reson Med* 2005; 54: 87–95.
  18. Haacke EM, Cheng NYC, House MJ, et al. Imaging iron stores in the brain using magnetic resonance imaging. *Magn Reson Imaging* 2005; 23: 1–25.
  19. Chiarelli PA, Bulte DP, Wise R, et al. A calibration method for quantitative BOLD fMRI based on hyperoxia. *NeuroImage* 2007; 37: 808–820.
  20. Chen JJ and Pike GB. Global cerebral oxidative metabolism during hypercapnia and hypocapnia in humans: implications for BOLD fMRI. *J Cereb Blood Flow Metab* 2010; 30: 1094–1099.
  21. Halani S, Kwinta JB, Golestani AM, et al. Comparing cerebrovascular reactivity measured using BOLD and cerebral blood flow MRI: The effect of basal vascular tension on vasodilatory and vasoconstrictive reactivity. *NeuroImage* 2015; 110: 110–123.
  22. Hyder F, Herman P, Sanganahalli BG, et al. Role of ongoing, intrinsic activity of neuronal populations for quantitative neuroimaging of functional magnetic resonance imaging-based networks. *Brain Connect* 2011; 1: 185–193.
  23. Logothetis NK. What we can do and what we cannot do with fMRI. *Nature* 2008; 453: 869–878.
  24. Van Zijl PC, Eleff SM, Ulatowski JA, et al. Quantitative assessment of blood flow, blood volume and blood oxygenation effects in functional magnetic resonance imaging. *Nat Med* 1998; 4: 159–167.
  25. Xu F, Ge Y and Lu H. Noninvasive quantification of whole-brain cerebral metabolic rate of oxygen (CMRO<sub>2</sub>) by MRI. *Magn Reson Med* 2009; 62: 141–148.
  26. Haacke EM and Reichenbach JR. *Susceptibility weighted imaging in MRI: Basic concepts and clinical applications*. Hoboken, NJ: Wiley-Blackwell, 2011.
  27. Tang J, Liu S, Neelavalli J, et al. Improving susceptibility mapping using a threshold-based K-space/image domain iterative reconstruction approach. *Magn Reson Med* 2013; 69: 1396–1407.
  28. Haacke EM. *Magnetic resonance imaging: Physical principles and sequence design*. New York, NY: Wiley-Liss, 1999.
  29. Detre JA, Zhang W, Roberts DA, et al. Tissue specific perfusion imaging using arterial spin labeling. *NMR Biomed* 1994; 7: 75–82.
  30. Edelman RR, Siewert B, Darby DG, et al. Qualitative mapping of cerebral blood flow and functional localization with echo-planar MR imaging and signal targeting with alternating radio frequency. *Radiology* 1994; 192: 513–520.
  31. Haacke EM, Liu S, Buch S, et al. Quantitative susceptibility mapping: current status and future directions. *Magn Reson Imaging* 2015; 33: 1–25.
  32. Zheng W, Nichol H, Liu S, et al. Measuring iron in the brain using quantitative susceptibility mapping and X-ray fluorescence imaging. *NeuroImage* 2013; 78: 68–74.
  33. Koch KM, Papademetris X, Rothman DL, et al. Rapid calculations of susceptibility-induced magnetostatic field perturbations for in vivo magnetic resonance. *Phys Med Biol* 2006; 51: 6381–6402.

34. Marques JP and Bowtell R. Application of a Fourier-based method for rapid calculation of field inhomogeneity due to spatial variation of magnetic susceptibility. *Concepts Magn Reson Part B Magn Reson Eng* 2005; 25B: 65–78.
35. Neelavalli J, Cheng Y-CN, Jiang J, et al. Removing background phase variations in susceptibility-weighted imaging using a fast, forward-field calculation. *J Magn Reson Imaging* 2009; 29: 937–948.
36. Mathew RJ and Wilson WH. Caffeine induced changes in cerebral circulation. *Stroke* 1985; 16: 814–817.
37. Cameron OG, Modell JG and Hariharan M. Caffeine and human cerebral blood flow: a positron emission tomography study. *Life Sci* 1990; 47: 1141–1146.
38. Sutherland GR, Peeling J, Lesiuk HJ, et al. The effects of caffeine on ischemic neuronal injury as determined by magnetic resonance imaging and histopathology. *Neuroscience* 1991; 42: 171–182.
39. Mulderink TA, Gitelman DR, Mesulam M-M, et al. On the use of caffeine as a contrast booster for BOLD fMRI studies. *NeuroImage* 2002; 15: 37–44.
40. Addicott MA, Yang LL, Peiffer AM, et al. The effect of daily caffeine use on cerebral blood flow: How much caffeine can we tolerate? *Hum Brain Mapp* 2009; 30: 3102–3114.
41. Chen Y and Parrish TB. Caffeine's effects on cerebrovascular reactivity and coupling between cerebral blood flow and oxygen metabolism. *NeuroImage* 2009; 44: 647–652.
42. Fujima N, Kudo K, Terae S, et al. Non-invasive measurement of oxygen saturation in the spinal vein using SWI: quantitative evaluation under conditions of physiological and caffeine load. *NeuroImage* 2011; 54: 344–349.
43. Rack-Gomer AL, Liao J and Liu TT. Caffeine reduces resting-state BOLD functional connectivity in the motor cortex. *NeuroImage* 2009; 46: 56–63.
44. Yamauchi H, Okazawa H, Kishibe Y, et al. The effect of acetazolamide on the changes of cerebral blood flow and oxygen metabolism during visual stimulation. *NeuroImage* 2003; 20: 543–549.
45. Hedera P, Lai S, Lewin JS, et al. Assessment of cerebral blood flow reserve using functional magnetic resonance imaging. *J Magn Reson Imaging* 1996; 6: 718–725.
46. Grossmann WM and Koeberle B. The dose-response relationship of acetazolamide on the cerebral blood flow in normal subjects. *Cerebrovasc Dis Basel Switz* 2000; 10: 65–69.
47. Okazawa H, Yamauchi H, Sugimoto K, et al. Effects of acetazolamide on cerebral blood flow, blood volume, and oxygen metabolism: a positron emission tomography study with healthy volunteers. *J Cereb Blood Flow Metab* 2001; 21: 1472–1479.
48. Haacke EM, Mittal S, Wu Z, et al. Susceptibility-weighted imaging: Technical aspects and clinical applications, part 1. *Am J Neuroradiol* 2009; 30: 19–30.
49. Ye Y, Hu J, Wu D, et al. Noncontrast-enhanced magnetic resonance angiography and venography imaging with enhanced angiography. *J Magn Reson Imaging* 2013; 38: 1539–1548.
50. Wang J, Aguirre GK, Kimberg DY, et al. Arterial spin labeling perfusion fMRI with very low task frequency. *Magn Reson Med* 2003; 49: 796–802.
51. Luh WM, Wong EC, Bandettini PA, et al. QUIPSS II with thin-slice T1I periodic saturation: a method for improving accuracy of quantitative perfusion imaging using pulsed arterial spin labeling. *Magn Reson Med* 1999; 41: 1246–1254.
52. Nöth U, Meadows GE, Kotajima F, et al. Cerebral vascular response to hypercapnia: determination with perfusion MRI at 1.5 and 3.0 Tesla using a pulsed arterial spin labeling technique. *J Magn Reson Imaging* 2006; 24: 1229–1235.
53. Ghiglia DC and Romero LA. Robust two-dimensional weighted and unweighted phase unwrapping that uses fast transforms and iterative methods. *J Opt Soc Am A* 1994; 11: 107–117.
54. Abdul-Rahman HS, Gdeisat MA, Burton DR, et al. Fast and robust three-dimensional best path phase unwrapping algorithm. *Appl Opt* 2007; 46: 6623–6635.
55. De Rochefort L, Liu T, Kressler B, et al. Quantitative susceptibility map reconstruction from MR phase data using Bayesian regularization: validation and application to brain imaging. *Magn Reson Med* 2010; 63: 194–206.
56. Wu D, Liu S, Buch S, et al. A fully flow-compensated multiecho susceptibility-weighted imaging sequence: The effects of acceleration and background field on flow compensation. *Magn Reson Med*. Epub ahead of print 5 September 2015. DOI: 10.1002/mrm.25878.
57. Wong EC, Buxton RB and Frank LR. A theoretical and experimental comparison of continuous and pulsed arterial spin labeling techniques for quantitative perfusion imaging. *Magn Reson Med* 1998; 40: 348–355.
58. Nehlig A, Daval JL and Debry G. Caffeine and the central nervous system: mechanisms of action, biochemical, metabolic and psychostimulant effects. *Brain Res Brain Res Rev* 1992; 17: 139–170.
59. Fantini S. A haemodynamic model for the physiological interpretation of in vivo measurements of the concentration and oxygen saturation of haemoglobin. *Phys Med Biol* 2002; 47: N249–N257.
60. Sedlacik J, Rauscher A and Reichenbach JR. Quantification of modulated blood oxygenation levels in single cerebral veins by investigating their MR signal decay. *Z Für Med Phys* 2009; 19: 48–57.
61. Jain V, Langham MC and Wehrli FW. MRI estimation of global brain oxygen consumption rate. *J Cereb Blood Flow Metab* 2010; 30: 1598–1607.
62. Ge Y, Zhang Z, Lu H, et al. Characterizing brain oxygen metabolism in patients with multiple sclerosis with T<sub>2</sub>-relaxation-under-spin-tagging MRI. *J Cereb Blood Flow Metab* 2012; 32: 403–412.
63. Donoho DL. Compressed sensing. *IEEE Trans Inf Theory* 2006; 52: 1289–1306.
64. Lustig M, Donoho D and Pauly JM. Sparse MRI: The application of compressed sensing for rapid MR imaging. *Magn Reson Med* 2007; 58: 1182–1195.
65. Candes EJ and Tao T. Near-optimal signal recovery from random projections: Universal encoding strategies? *IEEE Trans Inf Theory* 2006; 52: 5406–5425.
66. Hutchison RE, McPherson RA, Schexneider KI. Basic examination of blood and bone marrow. In: McPherson

- RA, Pincus MR (eds). *Henry's Clinical Diagnosis and Management by Laboratory Methods*. Philadelphia, PA: Elsevier Saunders; 2011: 512–513.
67. Uludağ K, Dubowitz DJ, Yoder EJ, et al. Coupling of cerebral blood flow and oxygen consumption during physiological activation and deactivation measured with fMRI. *NeuroImage* 2004; 23: 148–155.
  68. Wu CW, Gu H, Lu H, et al. Mapping functional connectivity based on synchronized CMRO<sub>2</sub> fluctuations during the resting state. *NeuroImage* 2009; 45: 694–701.
  69. Behzadi Y and Liu TT. Caffeine reduces the initial dip in the visual BOLD response at 3 T. *NeuroImage* 2006; 32: 9–15.
  70. Liu TT, Behzadi Y, Restom K, et al. Caffeine alters the temporal dynamics of the visual BOLD response. *NeuroImage* 2004; 23: 1402–1413.
  71. Field AS, Laurienti PJ, Yen Y-F, et al. Dietary caffeine consumption and withdrawal: confounding variables in quantitative cerebral perfusion studies? *Radiology* 2003; 227: 129–135.
  72. Perthen JE, Lansing AE, Liao J, et al. Caffeine-induced uncoupling of cerebral blood flow and oxygen metabolism: a calibrated BOLD fMRI study. *NeuroImage* 2008; 40: 237–247.
  73. Zhang J, Liu T, Gupta A, et al. Quantitative mapping of cerebral metabolic rate of oxygen (CMRO<sub>2</sub>) using quantitative susceptibility mapping (QSM). *Magn Reson Med* 2015; 74: 945–952.
  74. Vorstrup S, Henriksen L and Paulson OB. Effect of acetazolamide on cerebral blood flow and cerebral metabolic rate for oxygen. *J Clin Invest* 1984; 74: 1634–1639.